
# Organic charged polaritons in the ultrastrong coupling regime

# Organic charged polaritons in the ultrastrong coupling regime

Mao Wang,[1] Suman Mallick,[1] Anton Frisk Kockum,[2] and Karl Börjesson[1,*]
[1]*Department of Chemistry and Molecular Biology, University of Gothenburg, 412 96 Gothenburg, Sweden*
[2]*Department of Microtechnology and Nanoscience, Chalmers University of Technology, 412 96 Gothenburg, Sweden*

(Received 31 August 2021; revised 7 February 2022; accepted 1 March 2022; published 6 April 2022)

We embedded an all-hydrocarbon-based carbocation in a metallic microcavity that was tuned to resonance with an electronic transition of the carbocation. The measured Rabi splitting was 41% of the excitation energy, putting the system well into the ultrastrong coupling regime. Importantly, due to the intrinsic charge on the carbocation, the polaritons that form carry a significant charge fraction (0.55 $e_0$) and a large charge-to-mass ratio ($\sim$2400 $e_0/m_0$). Moreover, the ground state of the ultrastrongly coupled system is calculated to carry about 1% of one elementary charge. These unique properties of our system, together with its convenient preparation, provide a practical platform to study charged polaritons in the ultrastrong coupling regime.

DOI: 10.1103/PhysRevResearch.4.023016

## I. INTRODUCTION

Exciton-polaritons are hybrid light-matter quasiparticles formed when the electronic excitation in "matter" is strongly coupled to a resonant electromagnetic field. To reach the strong coupling regime, the coupling strength (i.e., half the Rabi splitting $\hbar\Omega$), which quantifies the light-matter coupling strength, must be larger than the overall dissipation of the system. When the coupling strength is further increased and approaches a significant fraction ($\gtrsim$10%) of the bare energy of the excitation ($E_x$), the system enters the so-called ultrastrong coupling (USC) regime [1–3]. In this regime, not only the excited state of the system, but also the ground state acquires photonic and excitonic contributions [1–4]. This change is due to the antiresonant contribution in the interaction, which is usually ignored in standard strongly coupled systems, and leads to a renormalization of the electromagnetic field [5–7]. Theoretical investigations show that the virtual photons in the ground state can be released by nonadiabatic manipulation of the coupling strength [8–16]. The new hybrid ground state may have modified attributes including ground-state chemical reactivity [17], ground-state electroluminescence [18], and electrical conductivity and optoelectrical properties [19,20].

The USC regime has been reached in several systems, including inorganic quantum well intersubband microcavities [21], superconducting circuits [22], organic molecules in metallic microcavities [23], plasmonic nanoparticles [24], etc. (a detailed list of systems can be found in Ref. [1]). Most of these systems demand precise fabrication or cryogenic conditions, which is challenging. More diverse and readily prepared systems are therefore needed in order to explore the new phenomena predicted in the USC regime and to move towards practical applications [25].

In this paper, we show how trions can be used to reach USC in a system that only requires relatively simple preparation. Trions are excitons containing an extra hole or electron. When trions are strongly coupled to cavity photons, the newly formed polaritons are expected to carry a fraction of a net charge [26,27]. Trions therefore enable direct manipulation of the polariton behavior with external electrical or magnetic fields. Furthermore, charged polaritons have a strong interaction among each other because of Coulomb interaction and therefore constitute a promising platform to observe nonlinear phenomena [28].

Trions are generally unstable and can easily decompose into an exciton and a free charge at room temperature. Charged polaritons were therefore first achieved in inorganic quantum wells inside a microcavity at liquid-helium temperatures [26,27]. It should be noted that the formation of trion polaritons did not affect the transport of charges in these systems. This can be explained because as the polariton oscillates between light and matter, the charge remains fixed in position. Later trions were realized by strongly coupling trions in electrically doped semiconducting single-walled carbon nanotubes to cavity photons [29]. However, the energy of trions in both inorganic quantum wells and nanotubes lies close to that of the neutral exciton. The formed charged polaritons are therefore always strongly admixed with the neutral exciton, making it challenging to study their intrinsic properties. For molecular systems, charged polaritons were recently reported by strongly coupling the electronic transition of hole-doped organic semiconductors in planar microcavities [30,31]. Here, an increase in photocurrent was observed and explained by an increase in the yield of dissociating Coulombically bound holes from their counterions. The coupled transition arises from electronic excitation from the lower-lying orbitals to the partially vacant highest occupied molecular orbital of the hole-doped molecules. This method establishes a path

*karl.borjesson@gu.se

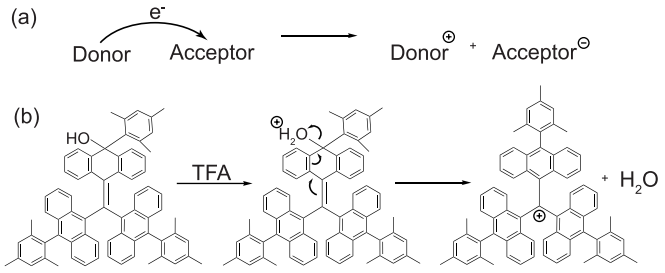


FIG. 1. (a) Conventional doping using an electron transfer reaction from a donor to an acceptor molecule. (b) Protonation using trifluoroacetic acid (TFA) followed by water elimination leading to the tris(10-mesitylanthr-9-yl)methyl cation (TAntM).

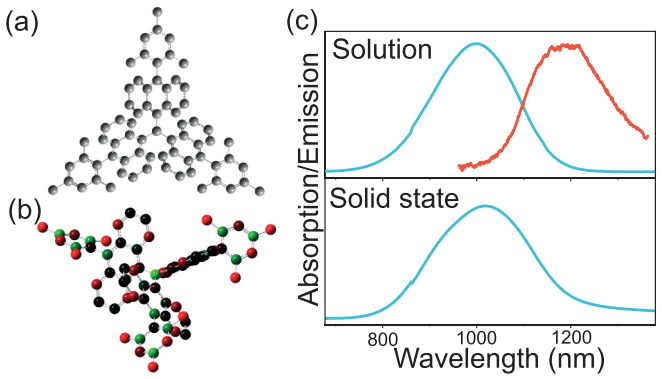


FIG. 2. (a) Top view of the crystal structure of TAntM showing the 120° binding angle of the central carbon. (b) Relative charge density map calculated by density functional theory showing atoms with partially positive charge as green and partially negative charge as red. (c) Absorption and emission of TAntM in TFA solution and the absorption of a spin-coated film of TAntM.

to achieve charged polaritons in molecules and opens the possibility to electrically tune polariton properties in organic semiconductors, although the doping ratio was not unity (30 wt %) and the highest possible collective coupling strength was therefore not achieved.

Here, we demonstrate room-temperature stable charged polaritons in the USC regime by strongly coupling the electronic transition of a carbocation to the optical field in a metallic Fabry-Pérot cavity. The carbocation carries an intrinsic net charge without extrinsic doping and can be regarded as a "100% doped" system. The obtained Rabi splitting can reach as high as ∼0.50 eV, amounting to 41% of the corresponding exciton energy (1.22 eV), which puts the system well into the USC regime. The charge-to-mass ratio of the lower polaritonic state is estimated to be three orders of magnitude higher than that of an electron. More importantly, the ground state of the system carries a net charge of 0.01 $e_0$ attributed to the effect of the USC. These unique properties of our system, together with its simple preparation, provide a practical platform to study charged polaritons in the USC regime.

## II. PHOTOPHYSICS OF THE CARBOCATION

In conventional chemical doping [Fig. 1(a)], an electron-transfer reaction occurs between the donor and acceptor molecules. In our system [Fig. 1(b)], the TAntM cation [tris(10-mesitylanthr-9-yl)methyl cation] was obtained by a two-step reaction: a proton transfer from trifluoroacetic acid (TFA) followed by an $H_2O$ elimination reaction [32]. This two-step reaction is irreversible as $H_2O$ is evaporated and the formed carbocation is therefore more stable than charged molecules formed by an electron-transfer reaction in the conventional doping method. Moreover, the formed carbocation, which usually is a chemically highly unstable species, is protected from nucleophilic attacks by the steric hindrance of the three surrounding bulky mesityl-substituted anthryl groups. These two effects result in unusually high stability for such an exotic molecule, allowing it to be handled under ambient conditions and solution processed into films.

The positive charge on TAntM is central to its photophysical properties. Firstly, the single-crystal x-ray structure of the molecule shows that the central carbon forms in-plane bonds having binding angles of 120° to the three bulky mesityl-substituted anthracene moieties [32]. Thus the central carbon is confirmed to be $sp^2$ hybridized [Fig. 2(a)]. Based on the electrostatic potential surface of the molecule calculated using density functional theory [Fig. 2(b)], the central carbon carries a fraction of a positive charge. In addition, other carbons in the molecule have a fractional positive charge (although smaller in comparison). These carbons can all be predicted from resonance structures of the Lewis structure in Fig. 1(b). The positive charge can therefore be considered somewhat delocalized over a considerable part of the molecule, increasing the chemical stability.

The characteristic feature of the absorption spectrum of the carbocation is an intense, broad band in the near-infrared regime [$\lambda_{max} = 990$ nm; Fig. 2(c)], with a peak molar absorption of $\sim 3.7 \times 10^4$ $M^{-1}$ $cm^{-1}$. This absorption band was assigned to the lowest-energy electronic transition ($S_1 \leftarrow S_0$), due to its mirror-image relationship to the emission spectrum. Emission was weak, close to the detection limit of the spectrofluorometer used in solution and undetectable in the solid state. Furthermore, time-dependent density-functional-theory calculations have previously predicted this transition to be, to a high degree, the result of a transition from the degenerate highest occupied molecular orbitals (HOMO and HOMO-1) to the lowest unoccupied molecular orbital (LUMO) [32]. The LUMO of the molecule contains the empty $p$ orbital of the positive central carbon, while the HOMOs were located on the surrounding anthracene moieties.

It is interesting to linger on the reason for the very low energy transition of the molecule, considering the small size of the aromatic network. The energy of the LUMO orbital is as low as −5.81 eV, a value comparable to the energy of the HOMO of many organic chromophores [32]. The reason for this low energy should be the empty $p$ orbital on the central carbon, and the reason why a molecule having such a high electron affinity can be stable at all should be the bulkiness of the anthracene units that protects the central carbon from nucleophilic attacks. The anthracene bulk physically protects the $p$ orbital of the central carbon, resulting in increased stability kinetically, and provides an energetic penalty for the central carbon to adopt a tetrahedral geometry resulting in increased stability thermodynamically. This class of dye, having

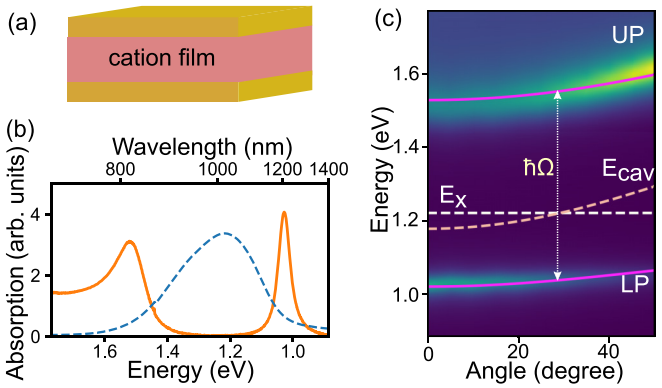


FIG. 3. (a) The cavity structure: 22 nm Au/270–300 nm TAntM film/22 nm Au. (b) The absorption of a carbocation film outside (blue dashed line) and inside the cavity (orange solid line). (c) The angular dispersion of the transmission spectra of a carbocation cavity. The purple solid lines are polaritonic branches obtained by fitting with the full Hopfield Hamiltonian, and the white and orange dashed lines are the exciton ($E_x$) and cavity ($E_{\mathrm{cav}}$) energies, respectively. LP and UP, lower and upper polariton, respectively.

an empty carbon $p$ orbital, contains a positive charge on the LUMO and may furthermore even represent a direction towards closed-shell organic dyes having electronic transitions approaching vibrational energies. In summary, the molecular exciton formed can be regarded as a positive trion: one exciton bound to a positive charge. When this trion is strongly coupled to a cavity photon, the polaritons formed will therefore carry a fraction of the net charge.

Thin films of the carbocation were readily prepared by the spin-coating method. The envelope of absorption of the films was retained from the one in solution [Fig. 2(c)], suggesting that intermolecular interactions are weak. This point is important in the following discussion of the photophysics within the strong coupling regime, since it shows that each excited molecule can be regarded as an individual exciton. The peak absorption coefficient $\alpha$ of the film is $1.05 \times 10^5$ cm$^{-1}$. Based on the absorption cross section $\sigma = 6.14 \times 10^{-17}$ cm$^2$ derived from the molar absorption coefficient in solution, the charge density of the cation film is on the order of $10^{21}$ cm$^{-3}$, one order of magnitude higher than the density ($10^{20}$ cm$^{-3}$) in a previous report using extrinsic doping by coevaporation of matrix and dopant molecules [30]. As the coupling strength is proportional to the square root of the exciton density [33], this high concentration indicates that the carbocation can be expected to achieve a much larger coupling strength and has the potential to reach the USC regime.

## III. THE ULTRASTRONG COUPLING REGIME

To explore the (ultra)strong coupling regime, three metallic Fabry-Pérot cavities containing a carbocation film with variable thickness were fabricated (the data from one are shown in the main text, and the data from the other two are shown in Appendix B). The active film was readily prepared by the spin-coating method (details in Appendix B). The cavity structure is shown in Fig. 3(a). The active layer did not contain any polymer matrix, which otherwise is commonly used in the field. It therefore allowed the highest concentration possible and thus the largest collective light-matter coupling strength achievable using this molecule. A typical absorption spectrum of the cavity is shown in Fig. 3(b). The single absorption band of the bare film centered at 1.22 eV is replaced by two polaritonic branches centered at 1.02 and 1.52 eV.

On resonance, the energy difference between the two polaritonic branches is about 0.5 eV, amounting to 41% of the bare exciton energy (1.22 eV). This implies that the system is in the USC regime. In this regime, the rotating-wave approximation is not valid and the system should be treated using the full Hopfield Hamiltonian $H_{\mathrm{Hop}}$, where the antiresonant and diamagnetic terms should be included (see Ref. [1] for details).

The polaritonic energies $E$ are described analytically by the eigenvalues of $H_{\mathrm{Hop}}$, which can be obtained by solving the quadratic equation [19]

$$\left(E_{\mathrm{cav}}^2 - E^2\right)\left(E_x^2 - E^2\right) = (\hbar\Omega)^2 E_{\mathrm{cav}}^2, \tag{1}$$

where $E_x$ and $E_{\mathrm{cav}}$ are the energies of the bare exciton and cavity, respectively. Figure 3(c) displays the angle-resolved transmission [transverse electric (TE) mode]. The polaritons show an angular dispersive behavior, and a clear anticrossing feature is observed close to the exciton energy of the carbocation. By fitting the angular data to the results from the full Hopfield Hamiltonian, the obtained Rabi splitting is 0.50 eV, which leads to a normalized coupling strength $\eta = \hbar\Omega/2E_x$ of 0.2. Thus it confirms that the system is well into the USC regime. Notably, in the resonant case, the full treatment leads to an asymmetric anticrossing in which the polaritonic energies follow [19,34]

$$E_{\mathrm{UP/LP}} = \sqrt{E_x^2 + \left(\frac{\hbar\Omega}{2}\right)^2} \pm \frac{\hbar\Omega}{2}, \tag{2}$$

due to a combined effect of the antiresonant and diamagnetic terms. The energy of the lower polariton lies closer to the exciton energy at resonance ($E_x = E_{\mathrm{cav}}$) and becomes more matterlike compared with the case for the strong coupling regime [Fig. 3(c)]. This anomalous effect is proportional to the normalized coupling strength $\eta$ and becomes significant in the USC regime [2].

Another important feature of the USC regime is the appearance of a band gap of forbidden polariton energies, where no solution to Eq. (1) will fall [19,35–37]. The forbidden frequencies correspond to destructive interference between the electromagnetic field radiated by the electronic oscillations and the bare microcavity photon field. As shown in Fig. 4(a), the solid lines represent the polaritonic branches obtained from the solution of Eq. (1). A polaritonic gap $E_g$ of 130 meV is formed between the asymptotic lines of the upper and lower polaritonic dispersions [$E_g = (\hbar\Omega)^2/2E_x$]. The relative size of the gap ($E_g/E_x$) is proportional to $\eta^2$ and therefore only becomes significant in the USC regime. It can therefore also be regarded as a signature of the USC regime [36] and has been observed previously [19,35–37].

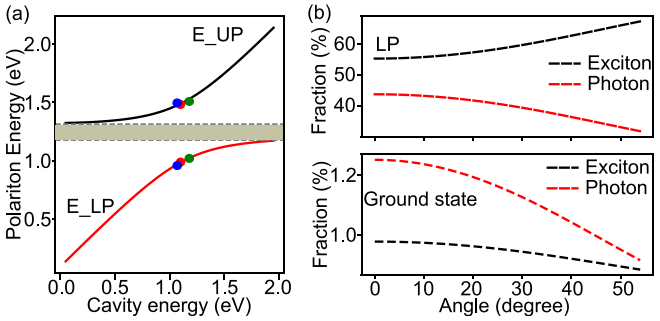


FIG. 4. (a) Polariton energy as a function of cavity energy. The solid lines are the simulated polariton dispersion, using the parameters obtained from the fit of the angular dispersive transmission spectra in Figs. 3(c), 8, and 9 with Eq. (1). The shaded region indicates the polariton gap. The blue, red, and green dots represent the polariton energies at $k = 0$ of the three studied cavities. (b) The photon and exciton ratios in the lower polariton (upper panel) and in the ground state (lower panel).

## IV. CHARGED POLARITON AND GROUND-STATE MODIFICATIONS

Polaritons that are composed of charged excitons are expected to carry a net electric charge that is equal to the electron charge $e_0$ times the relative fraction of the charged exciton in the polariton mode. For example, the effective charge of the lower polariton is

$$e_{\mathrm{eff,LP}} = e_0 |\alpha_{\mathrm{LP,ex}}|, \tag{3}$$

where $|\alpha_{\mathrm{LP,ex}}|^2$ is the exciton fraction of the lower polariton. This effective value represents the probability of finding an electron bound to the polariton. The charge-to-mass ratio $e/m$ is a key parameter for the transport behavior of charged species under an electrical field. The polariton effective mass is the weighted harmonic mean of the mass of its exciton and photon components,

$$\frac{1}{m_{\mathrm{eff,LP}}} = \frac{|\alpha_{\mathrm{LP,ex}}|^2}{m_{\mathrm{ex}}} + \frac{|\alpha_{\mathrm{LP,ph}}|^2}{m_{\mathrm{ph}}}, \tag{4}$$

where $m_{\mathrm{ex}}$ and $m_{\mathrm{ph}}$ are the effective exciton and cavity-photon mass, respectively. As $m_{\mathrm{ph}} \ll m_{\mathrm{ex}}$, the effective polariton mass therefore mainly depends on the mass of the cavity photon, which is on the order of $10^{-4}$ times the bare electron mass $m_0$ [38]. Due to this low effective mass, the charged polaritons therefore possess a much larger charge-to-mass ratio than typical charge carriers in organic semiconductors.

In a previous report on a charged inorganic polariton [27], the charge-to-mass ratio of polaritons was shown to be orders of magnitude larger than that of the free electron, and the enclosed theoretical calculations indicated a significantly higher drift velocity for the charged polaritons. Similar enhanced effects for charge transport were also discussed for trion-polaritons in semiconducting carbon nanotubes (CNTs) [29]. The resulting charge-to-mass ratio in CNTs was about 200 times higher than that of an electron or hole. In our system, the net charge of the polariton is higher than that in inorganic or CNT systems, since the polaritonic states have no contribution from any neutral excitons. At zero probing angle ($k_{\parallel} = 0$), $e_{\mathrm{eff,LP}}$ is about 0.55 $e_0$, and the effective charge-to-mass ratio $e_{\mathrm{eff,LP}}/m_{\mathrm{eff,LP}}$ of the charged polariton reaches a value of $\sim$2400 $e_0/m_0$ [$m_{\mathrm{eff,LP}}$ is calculated from Eq. (4)]. Moreover, the charge fraction of polaritons can be further increased by blue-detuning the cavity. The effective mass of electrons in organic semiconductors is generally large due to the strong localized charge and can reach as high as 25 times that of the bare electron mass [39]. Thus it is expected that charged polaritons will have several orders of magnitude higher charge-carrier mobility than typical charges in organic semiconductors. However, for organic electronics, the charge transport most often occurs in the ground state. Therefore the formation of polaritonic states will have no obvious effect on the charge transport. This explains why only little attention has been devoted towards enhanced charge transport of organic semiconductors in the strong coupling regime [40–43].

In the USC regime, the treatment of the system with the full Hopfield Hamiltonian not only gives a more accurate description of the dispersion relation but also indicates that the ground state is a squeezed vacuum state, which contains contributions from (virtual) photons and excitons. The effect of the photon contribution on the ground state was first discussed by Ciuti *et al.* [2], who proposed the possibility of extracting the virtual photons by modulating the coupling strength, which is reminiscent of the dynamical Casimir effect [44]. Later, Cirio *et al.* showed that electroluminescence can occur from the ground state in an ultrastrongly coupled system [18,45].

Here, we want to emphasize the effect of the exciton contribution on the polaritonic ground state. In our system, the uncoupled ground state carries a full positive charge. In the USC regime, the ground state will carry an additional certain fraction of charge inherited from the exciton component. The photon and exciton components in the lower polariton and the ground state are shown in the upper and lower panels of Fig. 4(b), respectively. In our red-detuned cavity, the energy of the cavity moves closer to the exciton energy as the angle increases and the LP becomes more excitonlike. However, both the excitonic and photonic contributions to the ground state decrease with increasing angle, a similar trend to that in a previous report of an ultrastrongly coupled system by Kéna-Cohen *et al.* [34]. At 0°, the exciton contribution to the ground state of the system is about 1%. In this sense, the ground state will carry a fractional charge of 0.01 $e_0$. It is up for discussion what the charge-to-mass ratio is for this fractional charge, although we expect it to be quite small. Of course, the ground state of the individual molecule is to the largest degree unperturbed. It is worth noting that this phenomenon only occurs when the charged polariton is in the USC regime, in which the ground state has a contribution from the charged excitons. Furthermore, how the fractional charge of the ground state could be interpreted in any change of eventual ground-state mass is open for discussion.

## V. CONCLUSION

We have demonstrated the formation of charged polaritons in the USC regime at room temperature using a simple planar metallic microcavity encapsulating a carbocation film. The strategy using a transition from a lower-lying orbital to the HOMO allowed for a very low exciton energy, resulting in the normalized coupling strength reaching as high as 20%, putting the system well into the USC regime. As a "100% doped" film, the formed polaritons can contain a significant charge fraction (0.55 $e_0$ for the lower polariton) and a large charge-to-mass ratio ($\sim$2400 $e_0/m_0$). Moreover, there is a reflection of the excited state into the ground state in the USC regime, allowing the ground state of the system to carry about 1% of the elementary charge $e_0$. It therefore implies the possibility of enhanced ground-state charge transport of organic materials in the USC regime through ground-state photoconductivity.

## ACKNOWLEDGMENTS

K.B. gratefully acknowledges financial support from the European Research Council (Grant No. ERC-2017-StG-757733), the Swedish Research Council (Grant No. 2016-03354), and the Knut and Alice Wallenberg Foundation (Grant No. KAW 2017.0192). A.F.K. acknowledges support from the Swedish Research Council (Grant No. 2019-03696) and from the Knut and Alice Wallenberg Foundation through the Wallenberg Centre for Quantum Technology (WACQT).

## APPENDIX A: SYNTHESIS

### 1. General

All starting materials were purchased from Sigma-Aldrich and used without further purification. All moisture- and oxygen-sensitive reactions were carried out using Schlenk techniques in oven-dried glassware. Solvents used for moisture- and oxygen-sensitive reactions were dried using an MBraun MB SPS-800 solvent purification system and, if necessary, degassed by freeze-pump-thaw cycles and stored over 4-Å molecular sieves under argon atmosphere. Flash chromatography was performed using a Teledyne CombiFlash EZ Prep system and normal-phase silica. $^1$H nuclear magnetic resonance (NMR) spectra were recorded on a Varian spectrometer at 400 MHz, J-coupling values are given in hertz, and chemical shifts are given in parts per million using tetramethylsilane, with 0.00 ppm as an internal standard.

The full synthesis scheme is shown in Fig. 5.

### 2. Synthesis of compound 3

2-bromomesitylene (425 mg, 2.12 mmol) was dissolved in dry tetrahydrofuran (THF; 15 ml) and cooled at −78 °C; then *n*-butyllithium (*n*-BuLi; 1.6 M hexane solution, 1.3 ml, 0.62 mmol) was added dropwise to the stirring solution. Compound 2 was prepared according to the literature procedure beforehand [32]. After stirring for 40 min at the same temperature, a solution of compound 2 (425 mg, 0.53 mmol) in dry THF (15 ml) was added and stirred for 3.5 h at room temperature. The reaction was monitored using thin-layer chromatography (TLC) and finally quenched by adding 5 ml water. The reaction mixture was extracted with dichloromethane (2 × 50 ml) and then washed with brine and dried over sodium sulfate. After removal of the solvent *in vacuo*, the crude material was purified by column chromatography on silica gel using dichloromethane and hexane as eluent to afford compound 3 (244 mg, 0.26 mmol, 53%) as a deep orange solid. NMR spectroscopy (see Fig. 6 and values below) values were in accordance with the literature [32].

Values of the $^1$H NMR [400 MHz, deuterated chloroform ($CDCl_3$)] spectra were as follows: $\delta$ 9.07 (dd, 2H, aromatic proton), 8.5d (dd, 2H, aromatic proton), 7.51–7.48

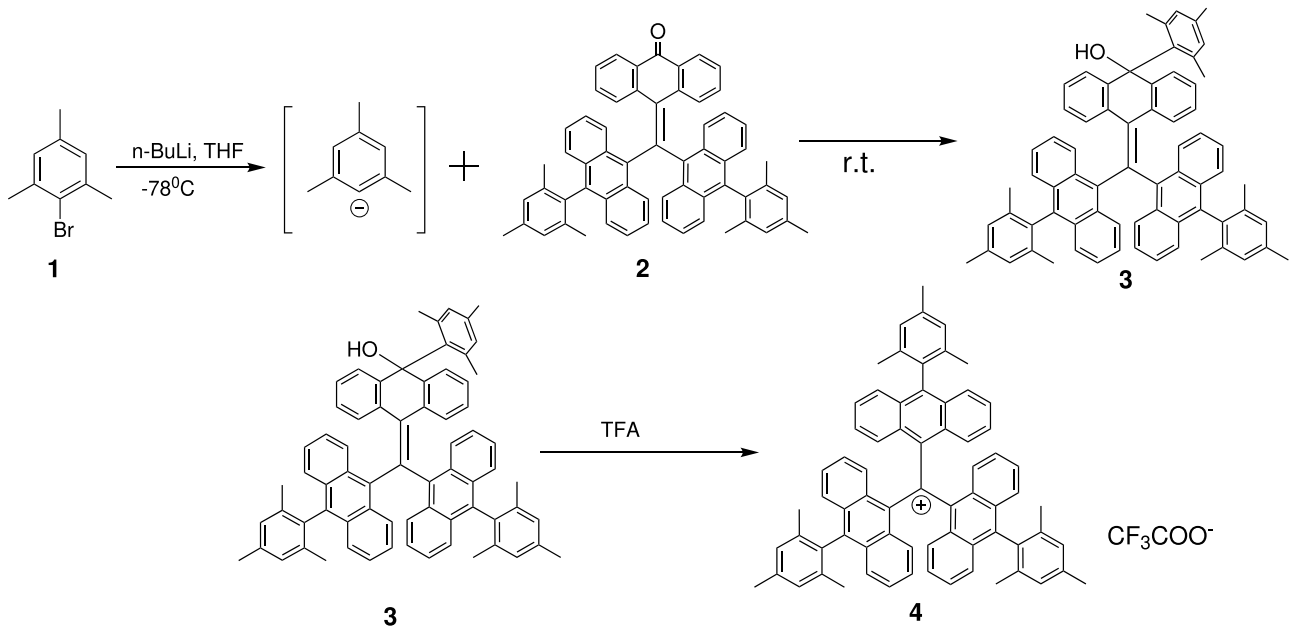


FIG. 5. Synthesis scheme. Here, r.t., room temperature.

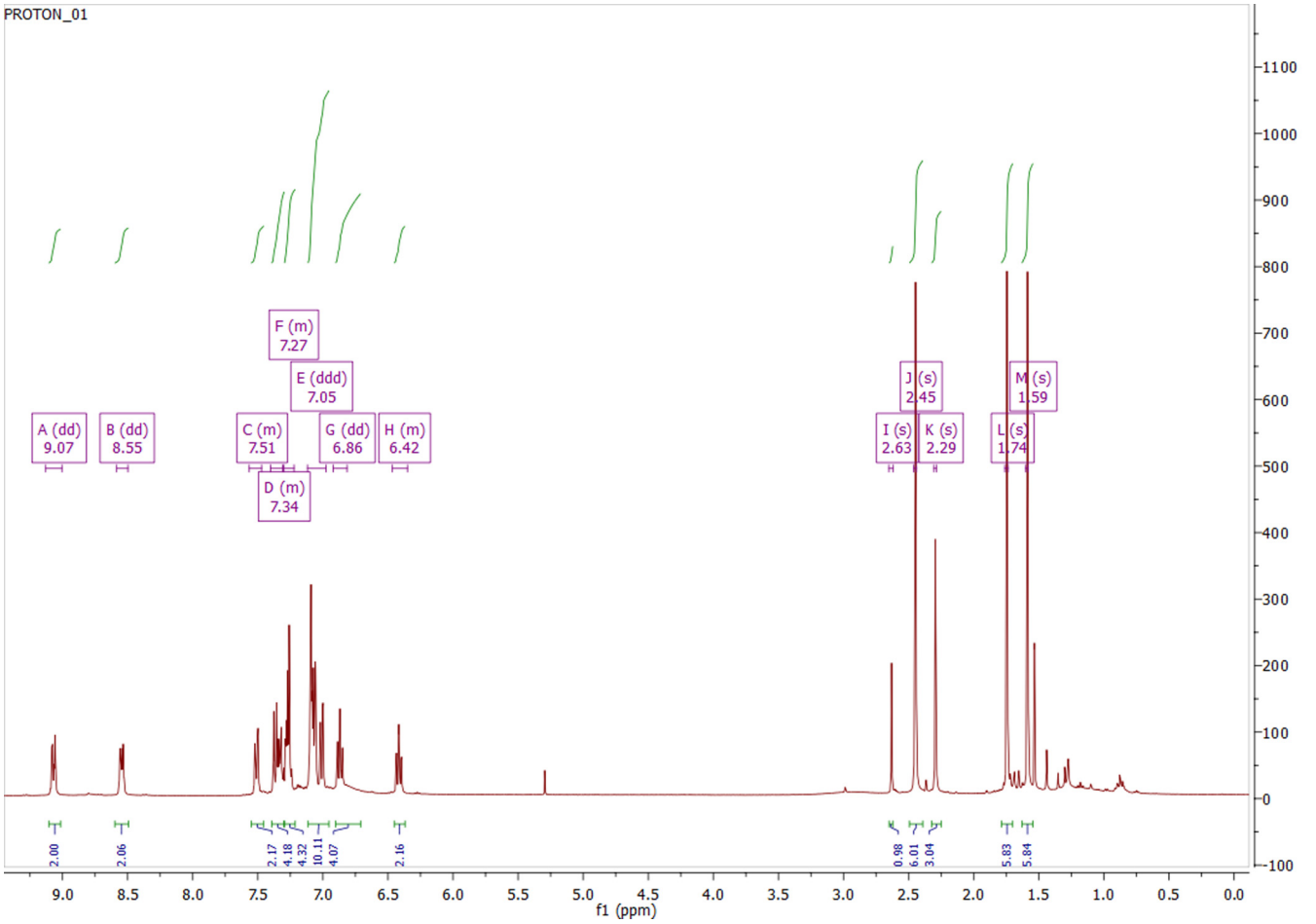


FIG. 6. $^1$H NMR spectra of the alcohol precursor used in the synthesis. See the text for extracted values.

(m, 2H, aromatic proton), 7.36–7.29 (m, 4H, aromatic proton), 7.27 (m, 4H, aromatic proton), 7.09–6.98 (m, 10H, aromatic proton), 6.90–6.60 (t + br, $J = 7.6$ Hz for t, 4H, aromatic proton), 6.42 (t, $J = 8.4$ Hz, 2H, aromatic proton), 2.62 (s, 1H, OH), 2.44 (s, 6H), 2.28 (s, 3H), 1.73 (s, 6H), 1.57 (s, 6H).

### 3. Synthesis of tris(10-mesitylanthr-9-yl)methyl cation (4)

Compound 3 (30 mg) obtained in the previous step was dissolved in 1 ml trifluoroacetic acid (TFA), and the solution was stirred for 2 min. The solution turned deep red in color, and the yield was quantitative, as evidenced by NMR spectroscopy (see Fig. 7), using TFA-d as the solvent.

Values of the $^1$H NMR (400 MHz, TFA-d) spectra were as follows: $\delta$ 8.28 (d, $J = 9.2$ Hz, 6H), 7.65 (d, $J = 8.8$ Hz, 6H), 7.28 (t, $J = 7.4$ Hz, 6H), 7.18 (s, 6H), 7.12 (m, 6H), 2.44 (s, 9H), 1.89 (s, 18H).

## APPENDIX B: CAVITY FABRICATION AND CHARACTERIZATION

Three dye-filled Fabry-Pérot cavities were manufactured. Au mirrors of the Fabry-Pérot cavities were fabricated by vacuum sputtering deposition (HEX, Korvus Technologies). A semitransparent Au (∼22 nm) film was sputtered on top of a precleaned glass substrate as the bottom mirror. Compound 3 (3.85 mg) was dissolved in trifluoroacetic acid (100 $\mu$l) to form the TAntM cation solution before spin-coating (1500 rpm) the film on the Au-covered substrates. The thickness of the film was measured by a calibrated KLA-Tencor Alpha-Step D-100 profilometer. The thicknesses of the TAntM film in the three cavities were 270, 290, and 300 nm. A top Au mirror (∼22 nm) was sputtered on the film to complete the cavity. Steady-state absorption spectra were measured using a standard spectrophotometer (Lambda 950, PerkinElmer). The angle-resolved transmission spectra were measured using the same spectrophotometer equipped with a rotatable sample holder. The results from these measurements are shown in Fig. 3(c) in the main text for the first cavity, while the results for the second and third cavities are shown in Figs. 8 and 9, respectively.

## APPENDIX C: QUANTUM-MECHANICAL CALCULATIONS

The Mulliken atomic charges were calculated using density functional theory using the GAUSSIAN 16 program package [46]. A ground-state energy calculation was performed using the geometry of the published crystal structure [32], the functional m06, and the basis set 6-311G+.

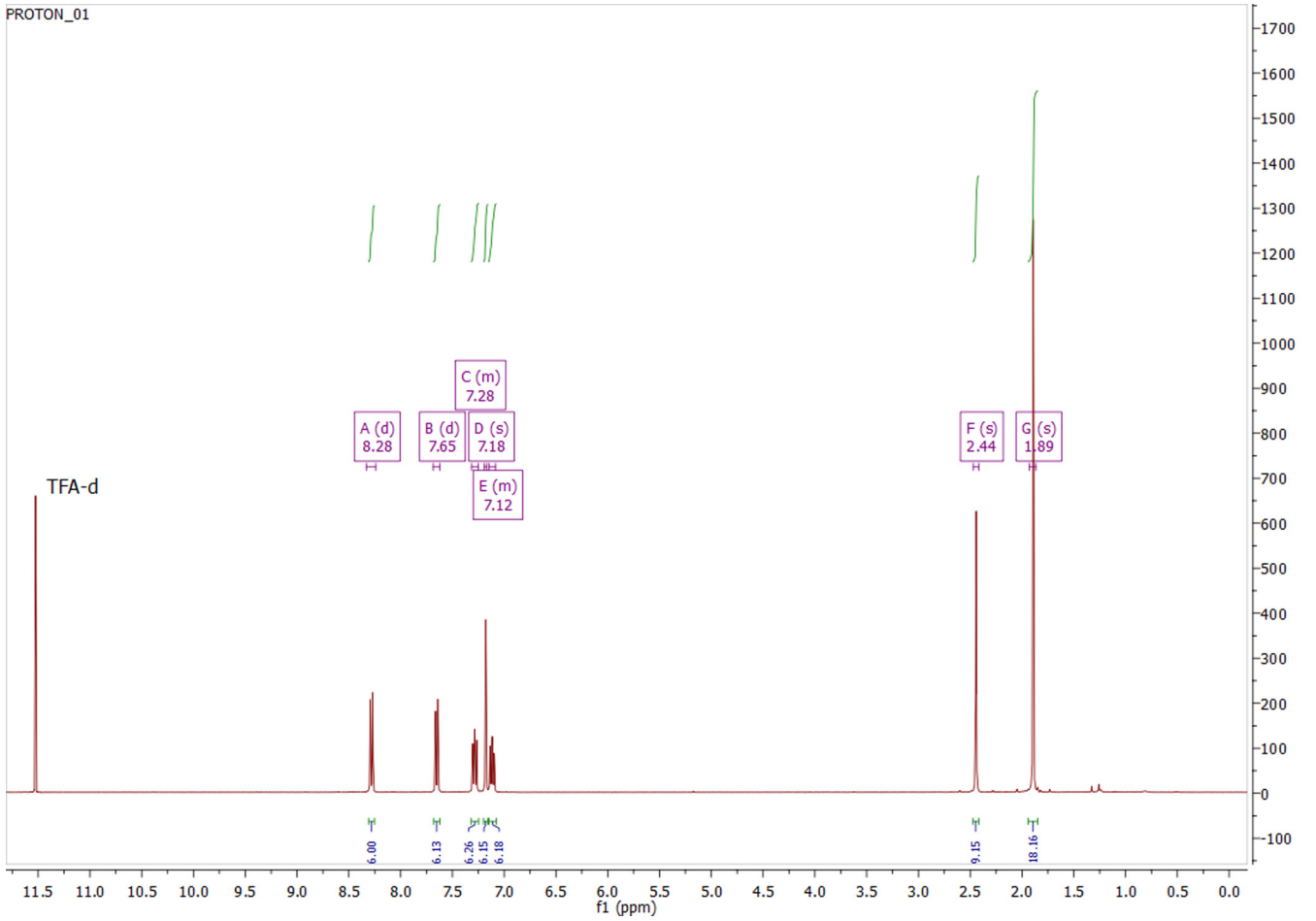


FIG. 7. $^{1}$H NMR spectra of the main product. See the text for extracted values.

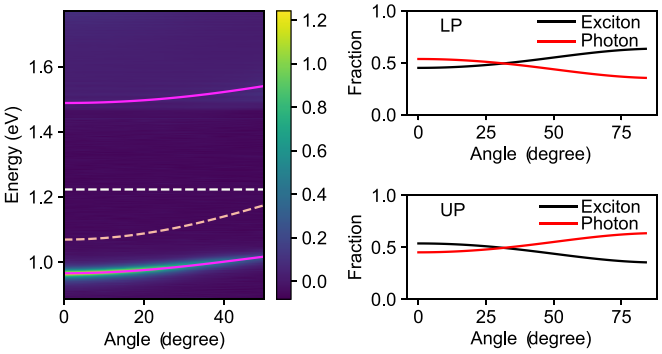


FIG. 8. The angular dispersion of the transmission spectra of a second carbocation cavity. The purple solid lines are polaritonic branches obtained by fitting with the full Hopfield Hamiltonian, and the dashed white and orange lines are the exciton ($E_x$) and cavity ($E_{\text{cav}}$) energies, respectively. At $k = 0$, the cavity energy is 1.07 eV, the detuning is $-0.15$ eV, and the fitted relative coupling strength is 20%.

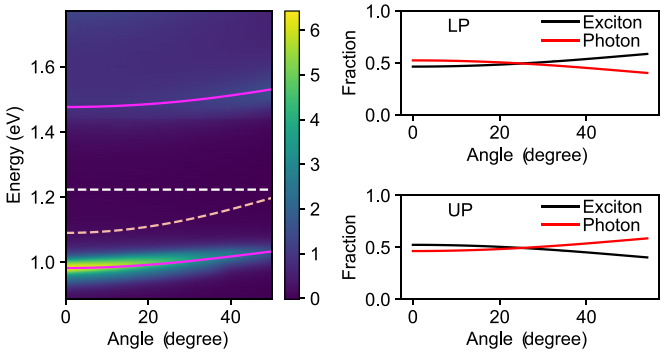


FIG. 9. The angular dispersion of the transmission spectra of a third carbocation cavity. The purple solid lines are polaritonic branches obtained by fitting with the full Hopfield Hamiltonian, and the dashed white and orange lines are the exciton ($E_x$) and cavity ($E_{\text{cav}}$) energies, respectively. At $k = 0$, the cavity energy is 1.10 eV, the detuning is $-0.13$ eV, and the fitted relative coupling strength is 20%.

[1] A. F. Kockum, A. Miranowicz, S. De Liberato, S. Savasta, and F. Nori, Ultrastrong coupling between light and matter, Nat. Rev. Phys. **1**, 19 (2019).

[2] C. Ciuti, G. Bastard, and I. Carusotto, Quantum vacuum properties of the intersubband cavity polariton field, Phys. Rev. B **72**, 115303 (2005).

[3] P. Forn-Díaz, L. Lamata, E. Rico, J. Kono, and E. Solano, Ultrastrong coupling regimes of light-matter interaction, Rev. Mod. Phys. **91**, 025005 (2019).

[4] S. Ashhab and F. Nori, Qubit-oscillator systems in the ultrastrong-coupling regime and their potential for preparing nonclassical states, Phys. Rev. A **81**, 042311 (2010).

[5] Y. Yu, S. Mallick, M. Wang, and K. Börjesson, Barrier-free reverse-intersystem crossing in organic molecules by strong light-matter coupling, Nat. Commun. **12**, 3255 (2021).

[6] C. Ye, S. Mallick, M. Hertzog, M. Kowalewski, and K. Börjesson, Direct transition from triplet excitons to hybrid light-matter states via triplet-triplet annihilation, J. Am. Chem. Soc. **143**, 7501 (2021).

[7] M. Wang, M. Hertzog, and K. Börjesson, Polariton-assisted excitation energy channeling in organic heterojunctions, Nat. Commun. **12**, 1874 (2021).

[8] G. Günter, A. A. Anappara, J. Hees, A. Sell, G. Biasiol, L. Sorba, S. De Liberato, C. Ciuti, A. Tredicucci, A. Leitenstorfer, and R. Huber, Sub-cycle switch-on of ultrastrong light–matter interaction, Nature (London) **458**, 178 (2009).

[9] S. De Liberato, C. Ciuti, and I. Carusotto, Quantum Vacuum Radiation Spectra from a Semiconductor Microcavity with a Time-Modulated Vacuum Rabi Frequency, Phys. Rev. Lett. **98**, 103602 (2007).

[10] F. Beaudoin, J. M. Gambetta, and A. Blais, Dissipation and ultrastrong coupling in circuit QED, Phys. Rev. A **84**, 043832 (2011).

[11] S. De Liberato, D. Gerace, I. Carusotto, and C. Ciuti, Extracavity quantum vacuum radiation from a single qubit, Phys. Rev. A **80**, 053810 (2009).

[12] K. Takashima, N. Hatakenaka, S. Kurihara, and A. Zeilinger, Nonstationary boundary effect for a quantum flux in superconducting nanocircuits, J. Phys. A: Math. Theor. **41**, 164036 (2008).

[13] T. Werlang, A. V. Dodonov, E. I. Duzzioni, and C. J. Villas-Bôas, Rabi model beyond the rotating-wave approximation: Generation of photons from vacuum through decoherence, Phys. Rev. A **78**, 053805 (2008).

[14] I. Carusotto, S. De Liberato, D. Gerace, and C. Ciuti, Back-reaction effects of quantum vacuum in cavity quantum electrodynamics, Phys. Rev. A **85**, 023805 (2012).

[15] L. Garziano, A. Ridolfo, R. Stassi, O. Di Stefano, and S. Savasta, Switching on and off of ultrastrong light-matter interaction: Photon statistics of quantum vacuum radiation, Phys. Rev. A **88**, 063829 (2013).

[16] D. S. Shapiro, A. A. Zhukov, W. V. Pogosov, and Y. E. Lozovik, Dynamical Lamb effect in a tunable superconducting qubit-cavity system, Phys. Rev. A **91**, 063814 (2015).

[17] F. Herrera and F. C. Spano, Cavity-Controlled Chemistry in Molecular Ensembles, Phys. Rev. Lett. **116**, 238301 (2016).

[18] M. Cirio, S. De Liberato, N. Lambert, and F. Nori, Ground State Electroluminescence, Phys. Rev. Lett. **116**, 113601 (2016).

[19] S. Gambino, M. Mazzeo, A. Genco, O. Di Stefano, S. Savasta, S. Patanè, D. Ballarini, F. Mangione, G. Lerario, D. Sanvitto, and G. Gigli, Exploring light–matter interaction phenomena under ultrastrong coupling regime, ACS Photonics **1**, 1042 (2014).

[20] B. Askenazi, A. Vasanelli, A. Delteil, Y. Todorov, L. C. Andreani, G. Beaudoin, I. Sagnes, and C. Sirtori, Ultra-strong light-matter coupling for designer Reststrahlen band, New J. Phys. **16**, 043029 (2014).

[21] A. A. Anappara, S. De Liberato, A. Tredicucci, C. Ciuti, G. Biasiol, L. Sorba, and F. Beltram, Signatures of the ultrastrong light-matter coupling regime, Phys. Rev. B **79**, 201303(R) (2009).

[22] T. Niemczyk, F. Deppe, H. Huebl, E. P. Menzel, F. Hocke, M. J. Schwarz, J. J. Garcia-Ripoll, D. Zueco, T. Hümmer, E. Solano, A. Marx, and R. Gross, Circuit quantum electrodynamics in the ultrastrong-coupling regime, Nat. Phys. **6**, 772 (2010).

[23] T. Schwartz, J. A. Hutchison, C. Genet, and T. W. Ebbesen, Reversible Switching of Ultrastrong Light-Molecule Coupling, Phys. Rev. Lett. **106**, 196405 (2011).

[24] N. S. Mueller, Y. Okamura, B. G. M. Vieira, S. Juergensen, H. Lange, E. B. Barros, F. Schulz, and S. Reich, Deep strong light-matter coupling in plasmonic nanoparticle crystals, Nature (London) **583**, 780 (2020).

[25] D. Sanvitto and S. Kéna-Cohen, The road towards polaritonic devices, Nat. Mater. **15**, 1061 (2016).

[26] R. Rapaport, R. Harel, E. Cohen, A. Ron, E. Linder, and L. N. Pfeiffer, Negatively Charged Quantum Well Polaritons in a GaAs/AlAs Microcavity: An Analog of Atoms in a Cavity, Phys. Rev. Lett. **84**, 1607 (2000).

[27] R. Rapaport, E. Cohen, A. Ron, E. Linder, and L. N. Pfeiffer, Negatively charged polaritons in a semiconductor microcavity, Phys. Rev. B **63**, 235310 (2001).

[28] K. S. Daskalakis, S. A. Maier, R. Murray, and S. Kéna-Cohen, Nonlinear interactions in an organic polariton condensate, Nat. Mater. **13**, 271 (2014).

[29] C. Möhl, A. Graf, F. J. Berger, J. Lüttgens, Y. Zakharko, V. Lumsargis, M. C. Gather, and J. Zaumseil, Trion-polariton formation in single-walled carbon nanotube microcavities, ACS Photonics **5**, 2074 (2018).

[30] C.-Y. Cheng, R. Dhanker, C. L. Gray, S. Mukhopadhyay, E. R. Kennehan, J. B. Asbury, A. Sokolov, and N. C. Giebink, Charged Polaron Polaritons in an Organic Semiconductor Microcavity, Phys. Rev. Lett. **120**, 017402 (2018).

[31] N. Krainova, A. J. Grede, D. Tsokkou, N. Banerji, and N. C. Giebink, Polaron Photoconductivity in the Weak and Strong Light-Matter Coupling Regime, Phys. Rev. Lett. **124**, 177401 (2020).

[32] T. Nishiuchi, S. Aibara, and T. Kubo, Synthesis and properties of a highly congested tri(9-anthryl)methyl radical, Angew. Chem., Int. Ed. **57**, 16516 (2018).

[33] M. Hertzog, M. Wang, J. Mony, and K. Börjesson, Strong light-matter interactions: a new direction within chemistry, Chem. Soc. Rev. **48**, 937 (2019).

[34] S. Kéna-Cohen, S. A. Maier, and D. D. C. Bradley, Ultrastrongly coupled exciton-polaritons in metal-clad organic semiconductor microcavities, Adv. Opt. Mater. **1**, 827 (2013).

[35] Y. Todorov, A. M. Andrews, R. Colombelli, S. De Liberato, C. Ciuti, P. Klang, G. Strasser, and C. Sirtori, Ultrastrong Light-Matter Coupling Regime with Polariton Dots, Phys. Rev. Lett. **105**, 196402 (2010).

[36] P. Jouy, A. Vasanelli, Y. Todorov, A. Delteil, G. Biasiol, L. Sorba, and C. Sirtori, Transition from strong to ultrastrong coupling regime in mid-infrared metal-dielectric-metal cavities, Appl. Phys. Lett. **98**, 231114 (2011).

[37] A. Delteil, A. Vasanelli, Y. Todorov, C. Feuillet Palma, M. Renaudat St-Jean, G. Beaudoin, I. Sagnes, and C. Sirtori, Charge-Induced Coherence between Intersubband Plasmons in a Quantum Structure, Phys. Rev. Lett. **109**, 246808 (2012).

[38] H. Deng, H. Haug, and Y. Yamamoto, Exciton-polariton Bose-Einstein condensation, Rev. Mod. Phys. **82**, 1489 (2010).

[39] V. Coropceanu, J. Cornil, D. A. da Silva Filho, Y. Olivier, R. Silbey, and J.-L. Brédas, Charge transport in organic semiconductors, Chem. Rev. (Washington, DC) **107**, 926 (2007).

[40] K. Nagarajan, J. George, A. Thomas, E. Devaux, T. Chervy, S. Azzini, K. Joseph, A. Jouaiti, M. W. Hosseini, A. Kumar, C. Genet, N. Bartolo, C. Ciuti, and T. W. Ebbesen, Conductivity and photoconductivity of a p-type organic semiconductor under ultrastrong coupling, ACS Nano **14**, 10219 (2020).

[41] E. Orgiu, J. George, J. A. Hutchison, E. Devaux, J. F. Dayen, B. Doudin, F. Stellacci, C. Genet, J. Schachenmayer, C. Genes, G. Pupillo, P. Samorì, and T. W. Ebbesen, Conductivity in organic semiconductors hybridized with the vacuum field, Nat. Mater. **14**, 1123 (2015).

[42] E. S. H. Kang, S. Chen, V. Derek, C. Hägglund, E. D. Głowacki, and M. P. Jonsson, Charge transport in phthalocyanine thin-film transistors coupled with Fabry-Perot cavities, J. Mater. Chem. C **9**, 2368 (2021).

[43] P. Bhatt, K. Kaur, and J. George, Enhanced charge transport in two-dimensional materials through light-matter strong coupling, ACS Nano **15**, 13616 (2021).

[44] G. T. Moore, Quantum theory of the electromagnetic field in a variable-length one-dimensional cavity, J. Math. Phys. (Melville, NY) **11**, 2679 (1970).

[45] M. Cirio, N. Shammah, N. Lambert, S. De Liberato, and F. Nori, Multielectron Ground State Electroluminescence, Phys. Rev. Lett. **122**, 190403 (2019).

[46] M. J. Frisch, G. W. Trucks, H. B. Schlegel, G. E. Scuseria, M. A. Robb, J. R. Cheeseman, G. Scalmani, V. Barone, G. A. Petersson, H. Nakatsuji, X. Li, M. Caricato, A. V. Marenich, J. Bloino, B. G. Janesko, R. Gomperts, B. Mennucci, H. P. Hratchian, J. V. Ortiz, A. F. Izmaylov *et al.*, *Gaussian 16 Revision C.01* (Gaussian Inc., Wallingford, CT, 2016).